Biomedical Optics EXPRESS

Pulsetrain-burst mode, ultrafast-laser interactions with 3D viable cell cultures as a model for soft biological tissues

Zuoming Qian,[1] Aghapi Mordovanakis,[1,2] Joshua E. Schoenly,[1] Andrés Covarrubias,[1] Yuanfeng Feng,[1] Lothar Lilge,[3] and Robin S. Marjoribanks[1,*]

[1] *Department of Physics, & Institute for Optical Sciences, University of Toronto, 60 St. George Street, Toronto ON M5S 1A7, Canada*

[2] *Current address: Biomedical Engineering, University of Michigan, 1101 Beal Avenue, Ann Arbor, Michigan 48109, USA*

[3] *Princess Margaret Hospital, Ontario Cancer Institute and Department of Medical Biophysics, University of Toronto, 610 University Ave., Toronto ON M5G 2M9, Canada*

[*] *marj@physics.utoronto.ca*

Abstract: A 3D living-cell culture in hydrogel has been developed as a standardized low-tensile-strength tissue proxy for study of ultrafast, pulsetrain-burst laser-tissue interactions. The hydrogel is permeable to fluorescent biomarkers and optically transparent, allowing viable and necrotic cells to be imaged in 3D by confocal microscopy. Good cell-viability allowed us to distinguish between typical cell mortality and delayed subcellular tissue damage (e.g., apoptosis and DNA repair complex formation), caused by laser irradiation. The range of necrosis depended on laser intensity, but not on pulsetrain-burst duration. DNA double-strand breaks were quantified, giving a preliminary upper limit for genetic damage following laser treatment.

OCIS codes: (170.1020) Ablation of tissue; (350.3390) Laser materials processing; (320.7090) Ultrafast lasers; (140.3440) Laser-induced breakdown; (160.1435) Biomaterials; (170.2520) Fluorescence microscopy.

References and links

1. T. Juhasz, H. Frieder, R. M. Kurtz, C. Horvath, J. F. Bille, and G. Mourou, "Corneal refractive surgery with femtosecond lasers," IEEE J. Sel. Top. Quantum Electron. **5**(4), 902–910 (1999).
2. I. Ratkay-Traub, I. E. Ferincz, T. Juhasz, R. M. Kurtz, and R. R. Krueger, "First clinical results with the femtosecond neodynium-glass laser in refractive surgery," J. Refract. Surg. **19**(2), 94–103 (2003).
3. P. Kim, G. L. Sutton, and D. S. Rootman, "Applications of the femtosecond laser in corneal refractive surgery," Curr. Opin. Ophthalmol. **22**(4), 238–244 (2011).
4. G. Sutton, S. J. Bali, and C. Hodge, "Femtosecond cataract surgery: transitioning to laser cataract," Curr. Opin. Ophthalmol. **24**(1), 3–8 (2013).
5. C. L. Hoy, W. N. Everett, M. Yildirim, J. Kobler, S. M. Zeitels, and A. Ben-Yakar, "Towards endoscopic ultrafast laser microsurgery of vocal folds," J. Biomed. Opt. **17**(3), 038002 (2012).
6. D. D. Lo, M. A. Mackanos, M. T. Chung, J. S. Hyun, D. T. Montoro, M. Grova, C. J. Liu, J. Wang, D. Palanker, A. J. Connolly, M. T. Longaker, C. H. Contag, and D. C. Wan, "Femtosecond plasma mediated laser ablation has advantages over mechanical osteotomy of cranial bone," Lasers Surg. Med. **44**(10), 805–814 (2012).
7. R. G. McCaughey, H. Sun, V. S. Rothholtz, T. Juhasz, and B. J. F. Wong, "Femtosecond laser ablation of the stapes," J. Biomed. Opt. **14**(2), 024040 (2009).
8. H. C. Yalcin, A. Shekhar, N. Nishimura, A. A. Rane, C. B. Schaffer, and J. T. Butcher, "Two-photon microscopy-guided femtosecond-laser photoablation of avian cardiogenesis: noninvasive creation of localized heart defects," Am. J. Physiol. Heart Circ. Physiol. **299**(5), H1728–H1735 (2010).
9. K. Kuetemeyer, G. Kensah, M. Heidrich, H. Meyer, U. Martin, I. Gruh, and A. Heisterkamp, "Two-photon induced collagen cross-linking in bioartificial cardiac tissue," Opt. Express **19**(17), 15996–16007 (2011).
10. F. Schelle, S. Polz, H. Haloui, A. Braun, C. Dehn, M. Frentzen and J. Meister, "Ultrashort pulsed laser (USPL) application in dentistry: basic investigations of ablation rates and thresholds on oral hard tissue and restorative materials," Laser Med. Sci. **2013**, 1–9 (2013)

#199036 - $15.00 USD Received 7 Oct 2013; revised 5 Dec 2013; accepted 7 Dec 2013; published 13 Dec 2013

11. M. H. Niemz, “Investigation and Spectral-Analysis of the Plasma-Induced Ablation Mechanism of Dental Hydroxyapatite,” Appl. Phys. B **58**(4), 273–281 (1994).
12. A. Vogel, J. Noack, G. Huttman, and G. Paltauf, “Mechanisms of femtosecond laser nanosurgery of cells and tissues,” Appl. Phys. B **81**(8), 1015–1047 (2005).
13. V. Nuzzo, I. Maxwell, S. Chung, E. Mazur and A. Heisterkamp, “Subcellular Surgery and Nanoneurosurgery Using Femtosecond Laser Pulses,” Nato. Sci. Peace Sec. B. **2011**, 203–218 (2011)
14. A. Tunnermann and J. Limpert, “Ultrafast Fiber Laser Technology: Status and Prospects,” Laser Resonators and Beam Control XII **7579**((2010)
15. P. S. Tsai, P. Blinder, B. J. Migliori, J. Neev, Y. Jin, J. A. Squier, and D. Kleinfeld, “Plasma-mediated ablation: an optical tool for submicrometer surgery on neuronal and vascular systems,” Curr. Opin. Biotechnol. **20**(1), 90–99 (2009).
16. A. Vogel and V. Venugopalan, “Mechanisms of pulsed laser ablation of biological tissues,” Chem. Rev. **103**(2), 577–644 (2003).
17. D. Manstein, G. S. Herron, R. K. Sink, H. Tanner, and R. R. Anderson, “Fractional photothermolysis: A new concept for cutaneous remodeling using microscopic patterns of thermal injury,” Lasers Surg. Med. **34**(5), 426–438 (2004).
18. D. Manstein and H.-J. Laubach, “Fractional Photothermolysis,” in Lasers in Dermatology and Medicine K. Nouri, Ed., pp. 123–147, Springer, New York (2011).
19. L. McKinney, F. Frank, D. Graper, J. Dean, P. Forrester, M. Rioblanc, M. Nantel, and R. Marjoribanks, “Mitigating Intrinsic Defects and Laser Damage using Pulsetrain-burst (>100 MHZ) Ultrafast Laser Processing,” Proc. SPIE **5970,** 14 (2005).
20. P. R. Herman, A. Oettl, K. P. Chen, and R. S. Marjoribanks, “Laser micromachining of 'transparent' fused silica with 1-ps pulses and pulse trains,” Comm. Biomed. Appl. Ultrafast Lasers. **3616**, 148–155 (1999).
21. R. R. Gattass, L. R. Cerami, and E. Mazur, “Micromachining of bulk glass with bursts of femtosecond laser pulses at variable repetition rates,” Opt. Express **14**(12), 5279–5284 (2006).
22. C. Dille, P. Kaifosh, P. Forrester, A. G. Mordovanakis, L. Lilge, and R. Marjoribanks, “Ablation of Hard Dental Tissue Using Ultrashort Pulsetrain-Burst (>100MHz) Laser,” in CLEO, p. JThE67, Optical Society of America, Baltimore, Maryland (2009).
23. R. R. Anderson, W. Farinelli, H. Laubach, D. Manstein, A. N. Yaroslavsky, J. Gubeli 3rd, K. Jordan, G. R. Neil, M. Shinn, W. Chandler, G. P. Williams, S. V. Benson, D. R. Douglas, and H. F. Dylla, “Selective photothermolysis of lipid-rich tissues: a free electron laser study,” Lasers Surg. Med. **38**(10), 913–919 (2006).
24. G. Edwards, R. Logan, M. Copeland, L. Reinisch, J. Davidson, B. Johnson, R. Maciunas, M. Mendenhall, R. Ossoff, J. Tribble, J. Werkhaven, and D. O’Day, “Tissue ablation by a free-electron laser tuned to the amide II band,” Nature **371**(6496), 416–419 (1994).
25. L. Reinisch and R. H. Ossoff, “Plasma ablation of hard tissue by the free-electron laser,” Proc. SPIE **1854** 145 (1993).
26. J. L. Drury and D. J. Mooney, “Hydrogels for tissue engineering: scaffold design variables and applications,” Biomaterials **24**(24), 4337–4351 (2003).
27. B. V. Slaughter, S. S. Khurshid, O. Z. Fisher, A. Khademhosseini, and N. A. Peppas, “Hydrogels in Regenerative Medicine,” Adv. Mater. **21**(32-33), 3307–3329 (2009).
28. M. A. El-Brawany, D. K. Nassiri, G. Terhaar, A. Shaw, I. Rivens, and K. Lozhken, “Measurement of thermal and ultrasonic properties of some biological tissues,” J. Med. Eng. Technol. **33**(3), 249–256 (2009).
29. V. Normand, D. L. Lootens, E. Amici, K. P. Plucknett, and P. Aymard, “New insight into agarose gel mechanical properties,” Biomacromolecules **1**(4), 730–738 (2000).
30. A. Vogel and V. Venugopalan, “Pulsed Laser Ablation of Soft Biological Tissues,” in *Optical-Thermal Reponse of Laser-Irradiated Tissue* A. J. Welch and M. J. C. van Gemert, Eds., (Springer Science + Business Media B. V. 2011), pp. 551–615.
31. K. R. Shull, “Materials Science: A Hard Concept in Soft Matter,” Nature **489**(7414), 36–37 (2012).
32. J. Y. Sun, X. H. Zhao, W. R. K. Illeperuma, O. Chaudhuri, K. H. Oh, D. J. Mooney, J. J. Vlassak, and Z. G. Suo, “Highly stretchable and tough hydrogels,” Nature **489**(7414), 133–136 (2012).
33. F. G. Pérez-Gutiérrez, S. Camacho-López, and G. Aguilar, “Time-resolved study of the mechanical response of tissue phantoms to nanosecond laser pulses,” J. Biomed. Opt. **16**(11), 115001 (2011).
34. A. V. Cherian and K. R. Rau, “Pulsed-laser-induced damage in rat corneas: time-resolved imaging of physical effects and acute biological response,” J. Biomed. Opt. **13**(2), 024009 (2008).
35. M. F. Ali, “Topical delivery and photodynamic evaluation of a multivesicular liposomal Rose Bengal,” Lasers Med. Sci. **26**(2), 267–275 (2011).
36. C. Sramek, L. S. Leung, T. Leng, J. Brown, Y. M. Paulus, G. Schuele, and D. Palanker, “Improving the therapeutic window of retinal photocoagulation by spatial and temporal modulation of the laser beam,” J. Biomed. Opt. **16**(2), 028004 (2011).
37. F. Xu, J. Celli, I. Rizvi, S. Moon, T. Hasan, and U. Demirci, “A three-dimensional in vitro ovarian cancer coculture model using a high-throughput cell patterning platform,” Biotechnol. J. **6**(2), 204–212 (2011).
38. R. Marjoribanks, C. Dille, J. E. Schoenly, L. McKinney, A. G. Mordovanakis, P. Kaifosh, P. Forrester, Z. Qian, A. Covarrubias, Y. Feng, and L. Lilge, “Ablation and thermal effects in treatment of hard and soft materials and biotissues using ultrafast-laser pulse-train bursts,” Photon. Lasers Med. **1**(3), 155–169 (2012).

#199036 - $15.00 USD Received 7 Oct 2013; revised 5 Dec 2013; accepted 7 Dec 2013; published 13 Dec 2013

39. R. Mocharla, H. Mocharla, and M. E. Hodes, "A novel, sensitive fluorometric staining technique for the detection of DNA in RNA preparations," Nucleic Acids Res. **15**(24), 10589 (1987).
40. M. J. Waring, "Complex Formation between Ethidium Bromide and Nucleic Acids," J. Mol. Biol. **13**(1), 269–282 (1965).
41. E. P. Rogakou, D. R. Pilch, A. H. Orr, V. S. Ivanova, and W. M. Bonner, "DNA Double-stranded Breaks Induce Histone H2AX Phosphorylation on Serine 139," J. Biol. Chem. **273**(10), 5858–5868 (1998).
42. N. Tinne, E. Lubking, H. Lubatschowski, A. Kruger and T. Ripken, "The influence of a spatial and temporal pulse-overlap on the laser-tissue-interaction of modern ophthalmic laser systems," Biomed. Tech. **57**(Suppl 1), 302–305 (2012)
43. Y. Gong, L. He, J. Li, Q. Zhou, Z. Ma, C. Gao, and J. Shen, "Hydrogel-filled polylactide porous scaffolds for cartilage tissue engineering," J. Biomed. Mater. Res. B Appl. Biomater. **82B**(1), 192–204 (2007).
44. J. P. Gong, Y. Katsuyama, T. Kurokawa and Y. Osada, "Double-network hydrogels with extremely high mechanical strength," Adv. Mater. **15**(14), 1155–1158 (2003)
45. N. K. Simha, C. S. Carlson, and J. L. Lewis, "Evaluation of fracture toughness of cartilage by micropenetration," J. Mater. Sci. Mater. Med. **15**(5), 631–639 (2004).
46. R. Gauvin, R. Parenteau-Bareil, D. Larouche, H. Marcoux, F. Bisson, A. Bonnet, F. A. Auger, S. Bolduc, and L. Germain, "Dynamic mechanical stimulations induce anisotropy and improve the tensile properties of engineered tissues produced without exogenous scaffolding," Acta Biomater. **7**(9), 3294–3301 (2011).
47. J. S. D'Souza, J. A. Dharmadhikari, A. K. Dharmadhikari, B. J. Rao, and D. Mathur, "Effect of Intense, Ultrashort Laser Pulses on DNA Plasmids in their Native State: Strand Breakages Induced by In Situ Electrons and Radicals," Phys. Rev. Lett. **106**(11), 118101 (2011).

1. Introduction

Ultrafast lasers (i.e., ≤1 ps pulse duration) have become practical and cost-effective in clinical environments as precise tools for delicate surgical procedures. Ever since they were first introduced for corneal flap creation [1, 2] in Laser-Assisted *in situ* Keratomileusis (LASIK), ultrafast lasers have become a standard resource in corneal refractive surgery [3] and an emerging tool for use in cataract surgery [4]. Extensive research aims to incorporate ultrafast lasers in various surgical procedures such as microsurgery of vocal folds [5], craniofacial osteotomy [6], stapedotomy [7], cardiology [8, 9], dentistry [10, 11], and sub-cellular nanosurgery [12, 13]. Continued increases in average powers for ultrafast fiber lasers [14] should eventually offer an even more compact and cost-effective alternative to solid-state ultrafast-laser systems.

Unlike long-pulse (i.e., >1 μs laser-pulse duration) laser ablation, which relies on linear absorption into endogenous chromophores (e.g., water), tissue ablation with ultrafast-laser pulses is plasma-mediated [12], offering submicrometer-scale precision [15], applicable over a broad range of tissues of varying optical and mechanical properties. Moreover, the collateral damage (e.g., cracking, charring) from ultrafast-laser ablation is small compared to most long-pulsed laser surgeries. This minimal collateral damage is due to the timescales of energy deposition and subsequent tissue ejection being much shorter than the timescales governing the propagation of laser-induced stresses and heat into the surrounding tissue [16]. Additionally, higher instantaneous intensities mean that the total energy density required to initiate ablation is lower for ultrashort pulses [12].

However, there are shortcomings when using ultrafast lasers as a surgical tool to ablate tissues. Typically the etch depths are shallow, resulting in slow removal rates and requiring higher repetition rates to reduce the total treatment time. Due to negligible thermal accumulation in the surrounding tissue after irradiation and ablation, the eschar region surrounding the ablation crater is small or non-existent. In general, a limited region of collateral damage (e.g., thermal coagulation) lining the incision is desired for homeostasis, sealing the open wound against the surrounding environment, preventing infection and, consequently, providing a more rapid wound-healing response. The method of fractional photothermolysis introduces new control by spatially partitioning the average therapeutic radiant exposure into microzone wounds, with regions of unaffected tissue between them [17, 18].

Ultrafast lasers operating in pulsetrain-burst mode at >100-MHz pulse-repetition rates offer a new mode of fluence delivery (fluence, or radiant exposure, has units of J/cm^2) that

#199036 - $15.00 USD Received 7 Oct 2013; revised 5 Dec 2013; accepted 7 Dec 2013; published 13 Dec 2013

increases material removal rates and controls accumulated heat from consecutive laser pulses, all while preserving the precise nature of ultrafast ablation. It has been shown in materials science applications that changing either the pulsetrain-burst duration, spacing between pulses, and/or pulse intensity can control melting in glass [19–21] and dental hard tissue [22]. Pulsetrain-burst delivery is also characteristic of free-electron lasers (FELs) [23–25], which typically generate a burst of picosecond pulses at very high repetition rates (> 1 GHz) within a macropulse of some microseconds duration. Wavelength tunability is the main advantage of FEL treatment of biotissue, but the interpulse timing within a macropulse, and macropulse duration, likely also govern the impact of FELs on materials and biotissues.

If this fluence-delivery method is applied to soft tissue ablation, altering the incident laser pulsetrain-burst parameters potentially provides control over the extent of eschar zone surrounding incision sites while minimizing other tissue damage mechanisms.

A standardized tissue model is largely desirable to determine the laser-operation parameters' impact on living biological systems following pulsetrain-burst mode ablation. Natural differentiated tissues are non-uniform, and have regions of connective or vascular tissue, which can complicate characterization of laser radiation impact. A tissue model for biophysics studies needs to be simple and homogeneous, so that cellular damage, from the expected primary damage mechanisms (thermal accumulation, shockwave disruptions and ionizing radiation), can be quantified spatially. Thermal accumulation and shockwaves can cause cellular necrosis and/or apoptosis, while ionizing radiation (extreme ultraviolet photons and Auger electrons) can cause single- or double-strand breaks of the DNA, leading to apoptosis, mutagenesis, or oncogenesis. The model needs to be biologically alive in order to see the evolution of subcellular tissue damage over time initiated by the laser pulse (e.g., apoptosis and DNA repair-complex formation). The tissue model also needs to be three dimensional (3D) to enable realistic modeling of not only laser energy deposition into the tissue model, but also the subsequent energy dissipation and propagation causing damage beyond the initial interaction zone (e.g., shockwaves and ionizing radiation), which must still be confined to the tissue phantom despite the potentially large effect volume. Additionally, the Young's modulus should also be representative of the target tissue's mechanical properties.

In terms of these criteria, proxy tissues offer a better standard model than *ex vivo* differentiated tissues do. Tissues taken *ex vivo* have limited cell-viability due to their large cell densities, versus low oxygen and nutrient delivery by diffusion. Low viability makes it impossible to characterize delayed cellular damage and death initiated by laser-irradiation.

While plated cell cultures can be appropriate as a tissue model to test the impact of laser ablation, such cultures are by definition two-dimensional, and cannot realistically model three-dimensional propagation damage (e.g., shockwaves) resulting from ultrafast laser exposure.

One possible option for a standard tissue model is a matrix of cross-linked polymer chains populated by viable cells, since the physical parameters (e.g., thermal and mechanical) of cross-linked polymer chains are homogeneous and scalable to match the Young's modulus of different tissues. Hydrophobic polymers are mechanically strong, but they are not suitable to encapsulate viable cells [26]. On the other hand, hydrogels (i.e., hydrophilic polymers) are frequently used as scaffolding materials for viable cells since they are processed under relatively mild conditions, are non-toxic to cells, and are permeable to oxygen and nutrients. Naturally derived hydrogel polymers (e.g., agar, alginate, and collagen) usually are either components of or have macromolecular properties similar to the extracellular matrix found in biological tissues [26, 27].

To be a suitable standard tissue model, the thermal and mechanical properties of the hydrogel should replicate those found in many biological tissues. These properties are important determining factors in the ablation mechanism and the resulting collateral cellular damage mechanisms. The thermal diffusivity of agar hydrogel is found to be comparable to

#199036 - $15.00 USD Received 7 Oct 2013; revised 5 Dec 2013; accepted 7 Dec 2013; published 13 Dec 2013

water and animal tissue (e.g., muscle, fat, and skin) [28]. Generally hydrogels have a limited ultimate tensile strength (UTS) and rupture easily, given that they lack a connective scaffold. Others [29] have found the UTS of agar-based hydrogels to be ~0.05 MPa – comparable to low tensile strength, high-water-content tissues like liver tissue [30]. However, some hydrogels have been synthesized with fracture toughness similar to cartilage [31, 32]. Hydrogels have been previously used as tissue proxies for laser-irradiation [33, 34] while hydrogel cell cultures are used in fundamental studies of cell response to drug and radiation treatments (e.g., photodynamic therapy [35] and interstitial laser photocoagulation [36] and can be adopted to represent appropriate tissue environments [37].

A 3D hydrogel comprising a living-cell culture was developed as a low tensile strength tissue proxy, permitting testing the impact of this novel modality of laser-ablation and understanding the extent of tissue damage for different laser parameters. The production of a 3D tissue proxy is reported with very good cell viability over long periods (~24 hours). Cellular damage (i.e., necrosis, apoptosis, and DNA double-stranded breaks) can be identified and quantified using commercial fluorescent biomarker assays followed by confocal fluorescence laser scanning microscopy (CFLSM). The tissue proxy is shown to be permeable to these small labeling fluorophores and can be virtually sectioned using CFLSM. Quantification of the extent of necrosis and DNA double-strand breaks (DSBs) following ultrafast pulsetrain-burst mode laser ablation at several laser parameters (i.e., per-pulse intensity and burst duration) demonstrates the suitability of this tissue proxy. Additionally the ablated volume can be determined optically.

2. Materials and methods

2.1 Viable hydrogel preparation

F98 rat glioma cells acting as damage sensors were first cultured in Dulbecco's medium (DMEM-H21, GIBCO) supplemented with fetal bovine serum (FBS) and antibiotics (penicillin and streptomycin). Upon reaching ~80% confluency, cells were trypsinized and centrifuged at 1500 rpm for 5 minutes. The resulting cell pellet was re-suspended in 6 mL of Alpha MEM medium (GIBCO, without phenol red) supplemented with FBS and antibiotics. Phenol red is a broadband fluorophore and would contribute background noise in CFLSM images.

The hydrogel was prepared by dissolving solid agar (Agar Bacteriological (Agar No.1), OXOID, Nepean, ON) in distilled water to 25 μg/mL at 125 °C in an autoclave for 1 hour. Afterwards the agar solution was brought to a temperature of 55 to 60 °C. The agar-water solution (4 mL) was thoroughly mixed with the 6-mL cell solution at room temperature and poured into 35-mm Petri dishes for a final cell density from 1×10^6 to 3×10^6 cells/mL. This final cell concentration corresponds to a mean cell-to-cell separation of ~50 μm, providing both adequate spatial resolution between cells for CFLSM and appropriate diffusion of oxygen and nutrients throughout the gel to prevent cell starvation. The hydrogel-cell mixture was left to solidify at room temperature for 2 to 3 minutes. A viability assay showed that the cell viability was maintained for >93% of all gel-imbedded cells after solidification of the hydrogel-cell mixture, immediately post-production. Punch-hole biopsies, 6 mm in diameter and 3 mm thick, were extracted from the hydrogel for single pulsetrain-burst laser irradiation experiments. Control hydrogels were also prepared — handled identically to experimental gels, but not laser-irradiated. On average, 3 hydrogels were used each day of experiments and 3 biopsies were extracted from each gel.

2.2 Laser irradiation

Within one hour of preparation, the hydrogel biopsies were irradiated with a single pulsetrain-burst from a purpose-built, ultrafast Nd:glass laser (1 ps; $\lambda = 1053$ nm) producing ~30-μs-duration pulsetrain bursts at 133-MHz pulse repetition rate [38]. The experimental setup is

#199036 - $15.00 USD Received 7 Oct 2013; revised 5 Dec 2013; accepted 7 Dec 2013; published 13 Dec 2013

shown in Fig. 1. A Pockels cell '*N*-pulse selector', similar to a pulse picker, was used to select a 0.1 to 20-μs-duration sub-train of the pulsetrain-burst. A waveplate-polarizer attenuator controlled the pulse energy that exited the oscillator. The pulsetrain-burst was amplified in two consecutive four-pass amplifiers to reach a maximum per-pulse energy of ~30 ± 3 μJ (variability arising from the pulse-to-pulse fluctuation within the burst), and per-burst energies up to 80 mJ. The pulsetrain-burst duration and per-burst energy were measured using a calibrated fast photodiode (DET210, Thorlabs, Newton, NJ).

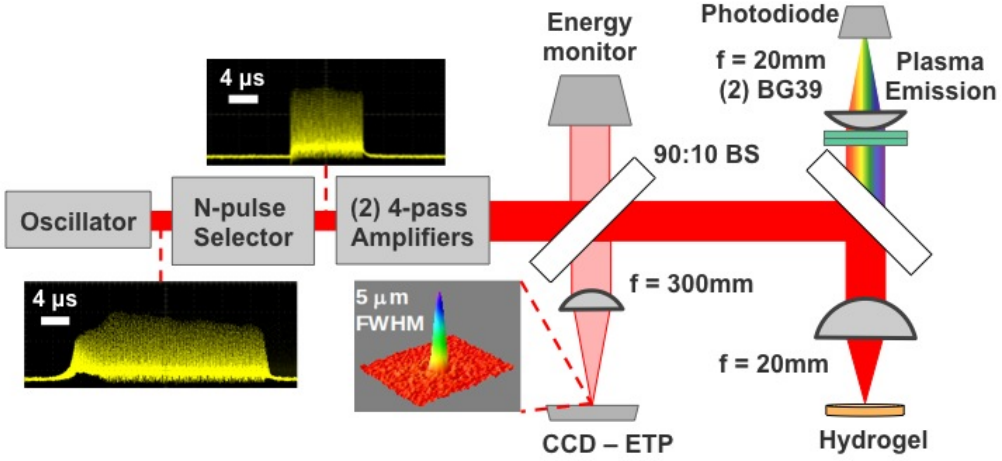

Fig. 1. Experimental setup for pulsetrain-burst mode laser ablation experiments. The oscilloscope traces show that the N-pulse selector selects a portion of the burst from the oscillator. This selected burst is amplified by two four-pass amplifiers and focused onto the target. A 90:10 beam splitter (BS) directs part of the oncoming laser light to an energy monitor and part of the laser light reflected from the target to an equivalent target plane (CCD-ETP). Relevant lens focal lengths are shown in the image.

The amplified pulsetrain-burst was focused onto the gel-sample surface using a 20-mm focal-length aspherical lens to a near-diffraction-limited ~5-μm-FWHM spot. At 30 μJ per pulse, the peak intensity at focus was 1.5×10^{14} W/cm^2. Laser light back-reflected from the gel surface was imaged with 15 × magnification onto a CCD camera, using a 300–mm focal length lens, to monitor the size and transverse profile of the focal spot. Each hydrogel biopsy was irradiated with just one pulsetrain-burst (shot) for characterization of the cellular response under a particular irradiation scheme.

2.3 Staining and confocal microscopy

After laser irradiation, the gel-biopsies were stained with fluorescent marker-dyes to tag different cells for examination under CFLSM. Hoechst 33342 (Invitrogen, Carlsbad, CA) was selected as a marker for all (viable, early-stage necrotic, and apoptotic) cells because it can permeate through intact and compromised cellular membrane [39] and intercalate with the DNA. Propidium iodide (PI; Invitrogen) was selected to mark only necrotic cells as it cannot penetrate across intact cellular membrane [40]. Similarly, Annexin-V (conjugated with fluorescein isothiocyanate (FITC); PHN1010, Invitrogen, Carlsbad, CA) was selected as biomarker for cells undergoing apoptosis. Annexin-V binds to phosphatidylserine localized on the cytosolic side of the plasma membrane, if this membrane is still intact. When cells undergo apoptosis, phosphatidylserine distributes across the inner and outer membranes, becoming accessible to Annexin-V. A mixture of 5-μg/mL Hoechst 33342 (0.616 kDa), 5-μg/mL propidium iodide (0.668 kDa), and 100-μL/mL Annexin-V (40 kDa) in binding buffer (Invitrogen, Carlsbad, CA) was added to the gel samples typically at 4 to 5 hours after laser

#199036 - $15.00 USD Received 7 Oct 2013; revised 5 Dec 2013; accepted 7 Dec 2013; published 13 Dec 2013

exposure. The hydrogels were stained at 5% CO_2 and 37°C for 1 hour, and afterwards washed with phosphate buffer solution (PBS).

An antibody staining method, γ-H2AX antibody (FITC conjugated; EMD Millipore, Billerica, MA), was used to tag DNA DSBs, since DSBs lead to Serine 139 phosphorylation on histone H2AX [41]. These hydrogel samples were first fixed in 4% paraformaldehyde at 4°C for ~12 hours, and cells permeabilized using 0.2% Triton X-100 (Sigma-Aldrich). After washing with 0.5% NP-40 (Sigma-Aldrich, St Louis, MO) and PBS, the fixed samples were stained with 1 mL of a preparation of 2-μg/mL γ-H2AX antibody (17 kDa) in a blocking solution of 4% bovine serum albumin and 4% goat serum in PBS. Subsequently, the samples were incubated at 4°C for 12 hours, and afterwards washed with PBS.

The distribution of fluorescently-tagged cells was mapped in 3D using a confocal laser scanning microscope (LSM 510, Zeiss, Jena, Germany) with an objective (10 × /0.5 N.A., FLUAR, Zeiss, Jena, Germany) having a 1.9-mm working distance, sufficient to access fluorophores 1.5-mm-deep within the hydrogel matrix. The fluorescence excitation (λ_{ex}) and emission (λ_{em}) wavelengths for each assay applied standard values: Hoechst 33324 (λ_{ex} = 400 nm, λ_{em} = 415 to 735 nm); PI (λ_{ex} = 488 nm, λ_{em} = 566 to 1000 nm); FITC-conjugated Annexin-V (λ_{ex} = 488 nm, λ_{em} = 493 to 1000 nm); FITC-conjugated γ-H2AX antibody (λ_{ex} = 488 nm, λ_{em} = 493 to 1000 nm). The typical volume scanned within the gel was 1 mm × 1 mm × 0.3 mm with ~1-μm-lateral and ~10-μm-depth increments. The lateral and axial resolution of the confocal fluorescence microscope at 700 nm, for example, was 0.6μm ($0.4\lambda_{em}$/N.A.) and 5.1μm ($1.4n\lambda_{em}$/N.A.^{2}), respectively, where n is the refractive index of the hydrogel (n≈1.3).

3. Results

The viability of cells was tested in control hydrogels for times up to 24 hours, corresponding to a time greater than the entire sequence of gel preparation, laser irradiation, staining and CFLSM analysis. Cells can lyse without laser irradiation due to extreme temperature during preparation or handling, by desiccation, or because of starvation of oxygen and nutrients. These 'incidentally necrotic' cells will add to the measured signal from PI staining of the laser-affected cells, possibly depending on depth below the surface. Punch-hole biopsy samples were extracted, in parallel with experimental samples, from hydrogels having cell densities of 1×10^6 and 3×10^6 cells/mL. These control samples were stained with Hoechst 33342 and PI at one, six, and twenty-four hours after initial gel preparation and analyzed by CFLSM. Irrespective of the cell densities prepared, and imaging depth, more than 90% of the embedded cells remain viable after 6 hours and more than 85% of the cells remain viable after 24 hours. A similar viable fraction (tagged only by Hoechst-33342) was also found in irradiated samples when scanning ~2 mm away from a laser-irradiated spot. These results demonstrate a high fraction of cells remain viable within the timeframe of laser-irradiation experiments and that the supply of oxygen and nutrients is sufficient.

#199036 - $15.00 USD Received 7 Oct 2013; revised 5 Dec 2013; accepted 7 Dec 2013; published 13 Dec 2013

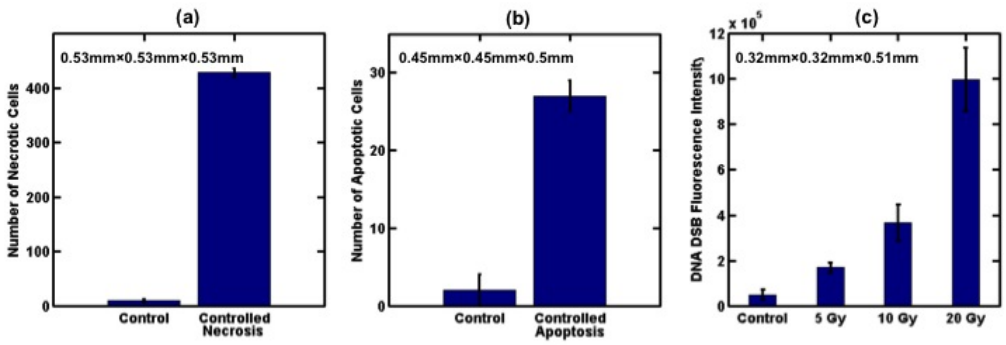

Fig. 2. Comparing the number of intentionally insulted cells within the hydrogel to those in a naïve control hydrogel. (a) Cellular necrosis induced by heating with a hot water bath. (b) Cellular apoptosis induced by cis-platin. (c) DNA double-stranded breaks (DSBs) induced by an X-ray source at various dosages. The dimension listed near the top of each plot is the volume scanned by the confocal microscope.

Figure 2 demonstrates the suitability of staining necrotic cells, apoptotic cells, and DNA DSBs within our 3D hydrogel cell culture. For each plot in Fig. 2, cells in hydrogel biopsies were intentionally insulted (i.e., thermal, chemical, and ionizing radiation), tagged by the appropriate biomarker, and compared to those cells tagged in a naïve control hydrogel. Cells were counted in the 3D CFLSM image by using a 3D cell counting macro in ImageJ (NIH, Bethesda, Maryland). Cells were counted in CFLSM images by first thresholding the measured fluorescence intensity per pixel at a minimum value, which rejected background noise without significantly rejecting fluorescence from cells, and then converting the image into a binary image. A median filter and a filter on the minimum cell size were also used to filter out shot noise.

Heating the hydrogel cell culture in a water bath at 65°C for ~10 min induced cellular necrosis in Fig. 2(a). Cellular apoptosis in Fig. 2(b) was induced by incubating the cells in 20mL of a 0.8mM cis-platin solution in DMEM for 5 hours, prior to seeding the cells into the hydrogel. Irradiating hydrogel cell cultures with a standard X-ray source (X-RAD 225Cx Micro IGRT, Precision X-ray, North Branford, CT) at 225 kVp, 13 mA, and ionizing doses from 5Gy to 20Gy induced DNA DSBs in Fig. 2(c). For all cases in Fig. 2, the intentionally insulted cells are clearly distinguished from those in the control hydrogel indicating the suitability of CFLSM and these biomarkers to detect these insults within this living cell culture in hydrogel.

The maximum depth of cells detected under CFLSM is shown in Fig. 3 for cells tagged by Hoechst 33342 in Figs. 3(a) and 3(b) and PI in Fig. 3(c). In Fig. 3(a), prior to mixing into the hydrogel, Hoechst 33342 tagged the cells *in vitro* whereas the cells in Figs. 3(b) and 3(c) were tagged *in situ* in the hydrogel, as described previously. Necrotic cells in Fig. 3(c) were intentionally insulted in the manner of the necrotic cells in Fig. 2(a). For all cases in Fig. 3, the cell count is relatively constant and independent of depth up to a maximum detectable depth of ~700 μm. Similar results were found for Annexin-V when tagging apoptotic cells in hydrogel. For the laser ablation experiments, the maximum depths scanned were 500 μm.

#199036 - $15.00 USD Received 7 Oct 2013; revised 5 Dec 2013; accepted 7 Dec 2013; published 13 Dec 2013

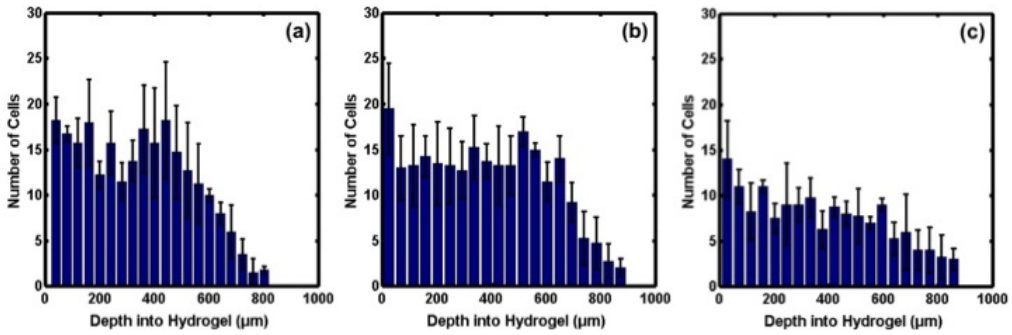

Fig. 3. The distribution of cells as a function of depth into the hydrogel, averaged over 4 field-of-views of 320μm × 320μm. (a) Cells tagged with Hoechst 33324 prior to seeding into the hydrogel. (b) Cells seeded into the hydrogel then tagged *post facto* with Hoechst 33342. (c) Necrotic cells within the hydrogel tagged *post facto* with PI. The cell count is relatively constant until a depth of ~700 μm from the hydrogel surface.

In principle, the maximum depth for detection of cells under CFLSM could be limited by optical scattering in the gel and the diffusion rate of fluorescent biomarkers, which in turn depends on their molecular weight. This maximum dateable depth depends upon the detectable fluorescence at deeper depths, which is shown for several biomarkers in Fig. 4. Cells marked by PI, Annexin-V, and γ-H2AX were intentionally insulted as for Fig. 2. As expected, the fluorescence intensity decreases with depth for all biomarkers as a result of optical scattering of the excitation and fluorescence within the hydrogel cell culture. The fluorescence intensity of dyes premixed into the hydrogel (Rhodamine-123 and Hoechst-33342) is slightly higher than those that permeated into the hydrogel, indicating that biomarker diffusion into the gel biopsies only slightly reduces the detectable fluorescence. This is supported by the similarity of the plots in Figs. 3(a) and 3(b), which also indicates that the diffusion rate of the biomarker is not limiting the maximum detectable depth.

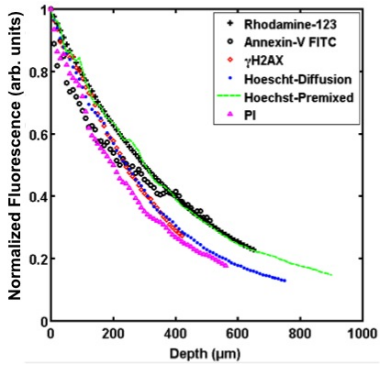

Fig. 4. The normalized fluorescence intensity detected from various biomarkers as a function of depth into the hydrogel. Each set of data traces is normalized to the maximum intensity of each trace. The fluorescence data for cells tagged by PI, Annexin-V, and γH2AX is from the controlled insult experiments found in Fig. 2. Fluctuations in the fluorescence intensity with depth may reflect the inhomogeneity of marked cells within a given hydrogel sample.

At greater depths, cell hypoxia and anoxia can result in widespread cellular apoptosis and inhibits cellular DNA repair mechanisms, limiting the maximum depth detected under γ-H2AX antibody staining. However, we have not observed any noticeable increase of apoptotic cells up to the maximum detectable depth of ~700 μm in control hydrogels for up to 24 hours and thus rule out this possibility.

The mechanical impact on the hydrogels after pulsetrain-burst mode laser ablation was investigated by measuring the dimensions of the ablation crater. In order to simplify the

#199036 - $15.00 USD Received 7 Oct 2013; revised 5 Dec 2013; accepted 7 Dec 2013; published 13 Dec 2013

confocal measurement, hydrogels prepared with Rhodamine-123, but without cells, were used. The crater dimensions were determined from CFLSM virtual sectioning. The shape of the ablation-crater was an oblate hemispheroid (Fig. 5(a)), where the crater volume (Fig. 5(b)) scaled nearly linearly with the per-pulse laser intensity over the range 0.05 – 1.0 × 10^{14} W/cm^2 but did not depend significantly upon the pulsetrain-burst duration between 0.5 and 10 μs. Ablation characteristics were found to be reproducible; with the data for Fig. 5 taken over experiments of 4 days using 24 gel biopsies.

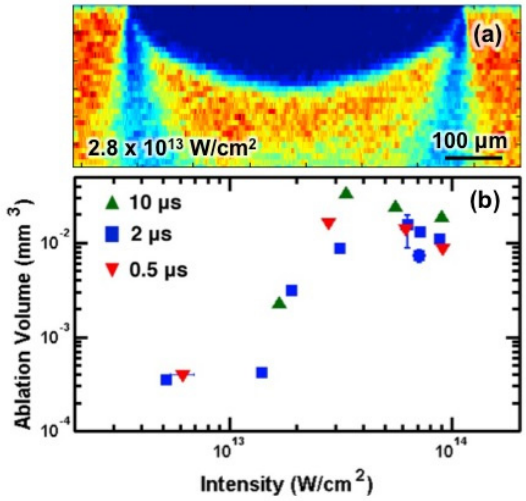

Fig. 5. (a) A lateral slice through an ablation crater in hydrogel as viewed under CFLSM. Voids at the crater edges are image artifacts, due to the steep edges of the crater. (b) The volume of the ablation crater in hydrogel as a function of per-pulse laser intensity at several pulsetrain burst durations.

The ablation crater volume was expected to increase with the pulsetrain burst duration, but the results in Fig. 5 suggest that ablation occurred only for the first handful of pulses in the pulsetrain. Based on the expectation that ablation is plasma-mediated, the plasma self-emission was measured using a 1-ns-risetime photodiode with two short-pass filters (BG39, Schott Glass) to attenuate the reflected 1053-nm laser light at an optical density of ~24. Consistently, the plasma self-emission in the visible-range of the spectrum was observed to last for ~100 ns regardless of pulsetrain-burst duration used down to the minimum achievable burst duration of 0.1 μs. This observation indicates that the leading 10 to 13 pulses solely contribute to plasma-mediated ablation of the hydrogel. This observation can be explained if the first 10 to 13 pulses vaporize sufficient water to explode in a bubble (i.e., explosive boiling), eventually ejecting material. This leaves a void in the gel extending over the focal volume, not permitting further absorption of laser radiation, leading to termination of the laser-plasma interaction. It has been shown elsewhere [42] that bubble formation stops absorption of successive laser pulses and subsequent ablation of water when using fs-laser-pulses, with repetition rates >1MHz.

Bubble formation in hydrogels during laser ablation follows explosive boiling of water. Rupture of the hydrogel is facilitated by its limited tensile strength. Higher tensile strength (e.g., where there is more connective tissue) would resist cavitation thereby permitting more pulses in a pulsetrain to interact with the dense tissue. Irradiating solid materials of higher tensile strength (e.g., glass or dental hard tissue) with pulsetrain bursts is seen to result in greater material removal with increasing burst duration [38], and to produce plasma self-emission throughout the entire burst.

#199036 - $15.00 USD Received 7 Oct 2013; revised 5 Dec 2013; accepted 7 Dec 2013; published 13 Dec 2013

The impact on cells following pulsetrain-burst mode laser ablation was determined by measuring the extent of cellular necrosis surrounding ablation craters using the assays combining Hoechst 33342 and PI in combination. The relative locations of both viable and necrotic cells in the CFLSM images were determined using a 3D cell counter macro in ImageJ. Following laser irradiation, the distribution of necrotic cells was roughly a hemisphere, approximately 100 to 250 μm in radius depending on pulse intensity. Taking the origin to be the point on the gel surface at the centre of this hemisphere, cells were binned by radius into equal-volume, hemispherical shells and counted (MATLAB (MathWorks)) (Fig. 6(a)). Within each of these bins, the number of viable and necrotic cells gave the necrosis fraction (i.e., the percentage of necrotic cells). To quantify the range of necrosis, this fraction was plotted as a function of distance from the origin and fitted with a smooth curve — we used a Gaussian function, being a smooth few-parameter fit relevant to thermal diffusion. The *necrosis range* was then taken to be the half-width at half-maximum of this distribution.

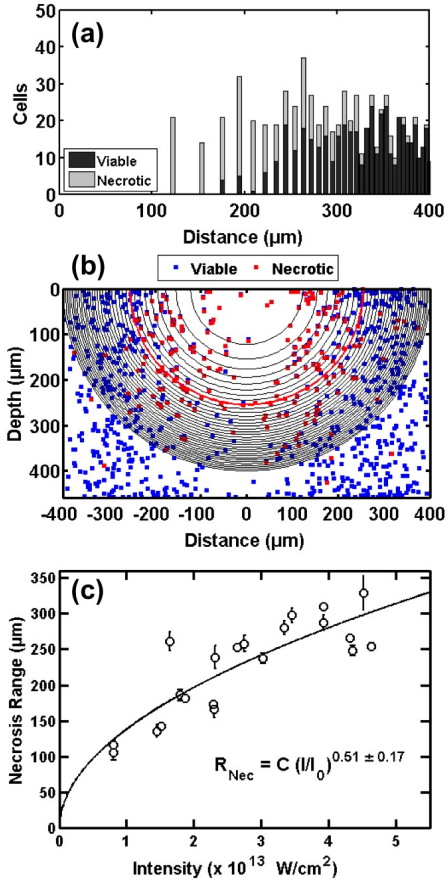

Fig. 6. (a) The number of viable and necrotic cells in hydrogel irradiated at a 4.6 × 10^{13}-W/cm^2 intensity and 1-μs-duration pulsetrain-burst as a function of distance from the centroid of the distribution of necrotic cells, but at the gel surface. Cells are binned in equal-volume, hemispherical shells. (b) Cylindrical projection of viable and necrotic cells, with hemispherical bins used for the analysis overlaid. The red hemisphere-line marks the necrosis range according to Gaussian fit. (c) The necrosis range as a function of the per-pulse laser intensity for a 1-μs-duration pulsetrain-burst. The line through the data points is a power-law fit with equation shown in the figure, where $I_0 = 1.0 \times 10^{13} W/cm^2$, and $C = 138 \pm 28 \mu m$. Error bars on data points are standard deviations multiple of Gaussian fits using different total number of hemispherical shells. Data shown was taken over 5 days of experiments from 5 separately produced gels providing 21 punch-hole gel biopsies.

#199036 - $15.00 USD Received 7 Oct 2013; revised 5 Dec 2013; accepted 7 Dec 2013; published 13 Dec 2013

Figure 6(b) presents a cylindrical projection of viable and necrotic cells, with the same hemispherical shells used for analysis. A few cells can be seen in the region where a crater is expected. One possible cause is the debris of necrotic cells floating from the surface of the crater into the liquid used for the assay. Another possible cause is that in the hydrogel, as for a soft tissue, the crater surface over several hours may slowly slump during staining and imaging. Rhodamine-123 allows for 3D measurement of the crater when using CFLSM (e.g., Fig. 5), but it cannot be combined with living cell cultures needed to measure necrosis range, since the dye itself is toxic. The live-dead assay liquid index-matches the hydrogel very well, preventing characterization of the crater shape during scanning, from the Fresnel reflectivity of the hydrogel free surface. Other ways to directly compare necrosis range and crater shape, in the same sample and at the same point in time, are being assessed.

The dependence of necrosis range on peak laser intensity, between 0.8×10^{13} and 4.6×10^{13} W/cm^2 for 1-μs-duration pulsetrain-bursts, is shown in Fig. 6(c). The necrosis range scales closely as $I^{1/2}$, the square root of the intensity.

The extent of cellular apoptosis surrounding ablation craters following laser ablation was also examined by an assay combining PI and Annexin-V. Three biopsies were irradiated at the highest laser intensity (1.5×10^{14} W/cm^2) over three separate days. Hydrogel cell cultures were investigated 6-8 hours following laser irradiation, since the collateral physical impact of ablation from pulsetrain bursts would most likely result in pre-programmed cell death. However, no apparent difference in cellular apoptosis was detected between irradiated and control hydrogels.

The feasibility of measuring DNA double-strand breaks in this hydrogel-culture proxy was evaluated by first irradiating viable-cell gels as control samples, using the commercial X-ray source described in connection with Fig. 2(c), and staining with a γ-H2AX antibody assay. In these control samples, we found we could clearly detect DNA double-strand breaks above background only for ionizing radiation doses to ~5 Gy. (This dose is for water, which has a density close to that of hydrogel (>95% water), but does not include absorption by the cells.) or greater. In the case of laser-irradiation at the highest-available peak-intensity (1.5×10^{14} W/cm^2), DNA double-strand breaks were not detectable above background. The γ-H2AX antibody assay depends on detection of the repair-complex formation in living cells — thus we conclude that if any cells received an ionizing-radiation dose of ~5Gy or greater, they were within the population of cells killed promptly or soon after; we did not detect viable cells with DNA double strand breaks due to pulsed laser ablation corresponding to this ionizing radiation dose.

4. Discussion/conclusion

Though studies on these viable hydrogel cell-cultures certainly do not replace studies on *ex vivo* and *in vivo* tissues, hydrogel cell-cultures do offer clear advantages as a standardized tissue model to study the biophysics of thermal, radiative, and shockwave phenomena in biotissue under ultrafast-laser ablation.

While most real tissues contain differentiated structures for support and transport, the homogeneity of hydrogels is an advantage when seeking to directly compare biophysics effects: the homogeneity of live-cell hydrogel proxies permits grater reproducibility of results. The hydrogel cell cultures in this study are also more permeable and less densely populated with cells compared to excised tissue; thus, cells located deep in a hydrogel remain viable over a longer period of time due to better gas and nutrient diffusion. This results in a low count of 'incidentally necrotic' cells causing 'noise', thus improving statistics in measurements of cellular damage from laser irradiation, compared to *ex vivo* tissue.

The permeability of hydrogel also permits fluorescent biomarkers to penetrate more easily into the hydrogel. Compared to excised natural tissues, this permits more rapid tagging of different cellular damage types (Fig. 2). The results in Figs. 2 and 3 demonstrate that

#199036 - $15.00 USD Received 7 Oct 2013; revised 5 Dec 2013; accepted 7 Dec 2013; published 13 Dec 2013

fluorescent biomarkers can be used successfully for quantitative analysis of these cellular deaths mechanisms in this standardized tissue model.

Hydrogel also has negligible optical absorption and little scattering in the visible, which make it well suited for optical virtual-sectioning methods, like CFLSM. Both this minimal attenuation of visible light, and the rapid diffusion of fluorescent biomarkers within the hydrogel, comes together to permit 3D imaging of laser-induced cellular damage deep within the sample (Figs. 3 and 4). To obtain similar 3D measurements of cellular damage in *ex vivo* tissue, microtome sectioning would be required. However, image-registration errors between slices are considerable, as thin slices have little structural integrity and may stretch or tear. Image-registration error is not an issue when using CFLSM to virtually section and image cellular insult in hydrogel cell cultures.

While our hydrogel tissue model, at present, does not reproduce the mechanical or dynamical characteristics of connective tissues (e.g., see a comparison of UTS in Table 1), different approaches are available which attempt to duplicate the mechanical properties of tissues in hydrogels. One method is to increase the agar concentration since it is generally proportional to the UTS [29]. Another technique, used to replicate cartilage tissue, is to embed the viable-cell hydrogel within a porous and mechanically strong scaffold (e.g., poly-L-lactide) [43]. Further, synthetic hydrogels containing double networks of long and short crosslinked polymers have been shown [31, 32, 44] to have high fracture toughness similar to cartilage [45]. Though not hydrogels, proxy tissues engineered by self-assembly and mechanically stimulated in a bioreactor have been developed with a UTS > 2MPa [46].

Table 1. The fracture stress and strain of 1% agarose hydrogel and various human biotissues.

	Fracture Stress (Tension, kPa)	Fracture Strain (Tension)
Agarose (1% w/w[a])	50	0.2
Tendon[b]	60,000	0.1
Cornea[b]	3,300	0.13
Skin[b]	13,000	0.6
Artery[b]	2,000	0.78
Liver[b]	29	0.44

[a]From [29]
[b]From [16]

While the above methods can approximate the mechanical characteristics of connective tissues in hydrogels, other useful properties such as optical transparency, cell biocompatibility, and biomarker permeability are compromised. For example, increasing the agar concentration of this hydrogel model also decreases the optical transparency and biomarker permeability. In this study we opted for the diagnostic advantages of this model.

For single-pulse or few-pulse ultrafast-laser interaction, the distinction between different tensile strengths may be unimportant — on such short timescales, inertial forces rather than the tissue's structural integrity may dominate mechanical dynamics. For ultrafast pulsetrain-burst interaction, however, it is shown here that 10-13 pulses opens a vapor bubble in the hydrogel around the focal location, which does not happen in hard tissues [38]; tissues with a collagen scaffold are expected to be an intermediate between these two.

In surgical applications, ultrafast pulsetrain-burst treatments are thought to offer control over the extent of the eschar zone around the laser-incision in tissue: by controlling the pulse-intensity envelope, or the duration of the pulsetrain burst, one can impact the surrounding tissue minimally (cf. single ultrafast pulses) or extensively (cf. long-pulses). Thus one could produce results using pulsetrain bursts that are intermediate between those produced from ultrafast and long laser pulses, or exploit individual advantages of each, as has been shown in solid-materials processing [38]. In hydrogels, explosive boiling and cavitation sets a limit on

#199036 - $15.00 USD Received 7 Oct 2013; revised 5 Dec 2013; accepted 7 Dec 2013; published 13 Dec 2013

the number of pulses that can be usefully applied in a pulsetrain-burst (Fig. 5), though the necrosis range can still be controlled through laser pulse intensity (Fig. 6(b)).

One of the principal outcomes of this study is the extent and nature of collateral damage caused by ultrafast-laser pulsetrain-burst interaction with live-culture hydrogels, for different parameters of the pulsetrain-burst. Cellular necrosis in biotissues is due to a combination of thermal diffusion and shockwave propagation. High repetition-rates lead to more rapid thermal accumulation and plasma-plume formation that may scald collateral cells, while shockwaves may create mechanical strain sufficient to rupture cellular membranes. For both mechanisms, the amount of damage is expected to increase with the temperature of the mediating plasma and the strength of the shockwave, which in turn increase with the per-pulse intensity. The increased extent of cellular necrosis with pulse intensity in Fig. 6 agrees with this expected scaling.

Different damage mechanisms should dominate when irradiating with either a single, ultrafast-laser pulse or a train of ultrafast-laser pulses. For single ultrafast-laser pulses, thermal damage should not play a large role in collateral cellular necrosis. For a long train of closely spaced ultrafast-laser pulses, thermal accumulation is a clear damage mechanism for the surrounding tissue [38]. However, it is unclear for viable-cell hydrogels as to whether absorption of 10-13 ultrafast pulses results in significant thermal accumulation, causing the range of cellular necrosis seen in Fig. 6. Also, the prospect of explosive boiling in hydrogels may mean that instead of 10 modest shockwaves, 10 pulses accumulate to create one large shockwave, particularly if material ejection is preceded by bubble formation.

For cells in a hydrogel matrix, irradiation with pulsetrain-bursts does not appear to result in widespread cellular apoptosis beyond the ablation crater. For pulsetrain-burst ultrafast-laser ablation, cellular apoptosis would likely result from the collateral physical impact of plasma-mediated ablation, such as heat and shockwaves, which would not activate death receptors and death signaling pathways through *de novo* protein synthesis (i.e., programmed cell death). Heat and/or shockwaves might rupture the mitochondrial membrane and lead to immediate release of cytochrome C, triggering a caspase cascade and result in pre-programmed cell death 6-8 hours after laser irradiation. However, for hydrogels irradiated with our laser, the immediate physical impact from ablation is strong enough to rupture the cellular membrane directly, causing cellular necrosis.

For cells in a hydrogel matrix, the preliminary results here indicate that ultrafast laser pulses delivered in pulsetrain bursts do not result in gross DNA double-strand breaking equivalent to 5Gy of absorbed dose — at least not in cells surviving long enough to activate the repair-complex mechanism. Possibly this result may not carry over to *in vivo* tissues: for instance, the relatively low concentration of metallic salts in hydrogels, compared to live tissue, may skew our result to lower doses of secondary radiation, since the flux and spectrum of XUV and X-ray photons depends sensitively on atomic number. It may also be that absorption of only 10-13 pulses in hydrogels produces plasma that is insufficient to produce appreciable DNA double-strand breaks, while much longer pulsetrain bursts may have greater effect. However, it is clear that more-sensitive measurements are needed, capable of detecting lower densities of DNA double-strand breaks at lower doses (<5 Gy) of ionizing radiation. Direct femtosecond-laser irradiation of DNA in aqueous solution at 12 TW/cm^2 (below the optical breakdown threshold of water) have been shown to result in DNA single-stranded breaks [47], but the results are likely to differ when DNA is located naturally within organelles inside cells that are embedded in a hydrogel matrix.

In conclusion, a 3D living cell culture was developed and shown to be a useful as a proxy for low tensile-strength tissues to study cellular response in biological tissues following ultrafast-laser ablation. Cells imbedded in gels are viable for extended times (> 85% viable after 24 hours) allowing time for biological response, cellular expression, and diffusion of a range of fluorescent cell markers. Tagged cells were found to be successfully imaged up to ~700 μm depth below the hydrogel surface, using virtual sectioning via confocal fluorescence

#199036 - $15.00 USD Received 7 Oct 2013; revised 5 Dec 2013; accepted 7 Dec 2013; published 13 Dec 2013

laser scanning microscopy. In application, the cell necrosis and apoptosis insult following pulsetrain-burst mode ultrafast laser ablation was characterized as a function of incident laser parameters. We expect this living tissue proxy to be well suited to fundamental studies of other therapeutic applications, such as photodynamic therapy, proton cancer therapy and X-ray irradiation.

Acknowledgments

This work was supported by the Natural Sciences and Engineering Research Council of Canada (NSERC).

#199036 - $15.00 USD Received 7 Oct 2013; revised 5 Dec 2013; accepted 7 Dec 2013; published 13 Dec 2013